(Received 29 May 2024, Accepted 19 June 2024, Scheduled 26 June 2024)

A Racket-Like UWB MIMO Antenna with High Isolation

Zhonggen Wang[1], Guoxiang Song[1,*], Wenyan Nie[2], Ming Yang[3], Chenlu Li[4], and Mingqing Wang[1]

[1]*School of Electrical and Information Engineering, Anhui University of Science and Technology, Huainan 232001, China*
[2]*School of Mechanical and Electrical Engineering, Huainan Normal University, Huainan 232001, China*
[3]*School of Electrical and Communications Engineering, West Anhui University, Lu'an 237012, China*
[4]*School Electrical and Information Engineering, Hefei Normal University, Hefei 230061, China*

ABSTRACT: In this paper, a dual-port ultra-wideband (UWB) MIMO antenna is proposed, featuring a highly compact structure with dimensions of only $25 \times 36 \times 1.6\,\text{mm}^3$. The designed antenna comprises two racket-shaped monopole antennas and a defective floor. Cross slots on the original T-shaped floor impede coupling current flow, significantly enhancing antenna isolation to achieve over 20 dB isolation across most frequency bands. The antenna operates at frequencies from $2.74 \sim 14.8$ GHz, meeting the stringent design criteria for UWB antennas. Furthermore, the diversity performance of the antenna is rigorously analyzed by simulating the envelope correlation coefficient (ECC), diversity gain (DG), total active reflection coefficient (TARC), and channel capacity losses (CCL). The designed antenna demonstrates excellent performance through comprehensive simulation and testing, showcasing its potential for applications in UWB MIMO systems.

1. INTRODUCTION

Antennas constitute vital components within contemporary communication networks and adept at transmuting electrical signals coursing through transmission lines into electromagnetic waves. The incessant evolution of communication technologies fosters an ever-expanding radio spectrum, thereby propelling advancements in UWB antenna technologies. The frequency band range for UWB antennas, designated by the U.S. Federal Communications Commission (FCC), spans from 3.1 to 10.6 GHz [1]. UWB antenna has a wide range of applications and can be used in wireless local area networks (LANs) due to its high transmission rate. It can also be used in radar and imaging, and in the medical field, it can provide high-resolution imaging solutions.

The integration of UWB and Multiple-Input-Multiple-Output (MIMO) technologies represents one of the most promising solutions for short-range wireless communication systems, offering expansive bandwidth, elevated data rates, mitigated multipath fading effects, and augmented capacity concurrently [2]. Continuous research on UWB MIMO antennas has led to numerous methodologies that enhance both the bandwidth and isolation of the antenna [3–22]. Ref. [3] details the design of a 4-element crescent-shaped double-sided MIMO antenna, employing patterning and polarization diversity techniques to ameliorate the isolation among its constituent elements. While the antenna attains an isolation of 20 dB across most frequency bands within a bandwidth of 12.4 GHz, its isolation diminishes to below 15 dB in the lower frequency bands, and it exhibits a relatively large size measuring $56\,\text{mm} \times 56\,\text{mm}$. Ref. [8] delineates the design of UWB and four-port MIMO antennas. The semicircular monopole patch undergoes modification through the inclusion of a guitar-shaped slot on the radiator and a half-circle slot in the lowered ground plane. The structural alteration influences the current path and improves impedance matching, consequently leading to a broader bandwidth. In [9], the design of an antenna integrates a T-like ground branch, serving as a decoupling structure. It consists of two modified inverted-L branches and an I-shaped stub, affording an isolation exceeding 20 dB across the entire operational bandwidth ($4.3 \sim 15.63$ GHz). In [11], a proposed antenna showcases a remarkable enhancement in isolation, reaching a maximum of 16 dB. This enhancement is achieved by incorporating a shared radiator with small rectangular slots, thereby effectively mitigating interference and enhancing overall performance. In [12], seven vertical metal barriers are introduced to the frontal aspect of an antenna, aiming to bolster the isolation between its two radiating elements. Ref. [13] introduces a four-port MIMO antenna characterized by an operational frequency range spanning 2.96 GHz to 13.2 GHz. The antenna is compact, measuring 56 mm by 56 mm, and achieves partial bandwidth and port isolation through a defective ground plane. In [14], the integration of an elliptical patch onto the original I-shaped ground plane is reported to enhance port isolation, as confirmed through eigenmode analysis. In [15], an antenna's bandwidth is broadened, and the inter-port decoupling is enhanced through the utilization of an inverted L-shaped defective ground plane. In [17], a two-port MIMO UWB antenna is introduced, operating within the frequency span of $3.1 \sim 13.5$ GHz, wherein the decoupling phenomenon is realized through the employment of an electromagnetic bandgap structure. The enhancement of antenna isolation by 10 dB relative to the scenario without an electromagnetic bandgap is observed. In [19], a UWB MIMO antenna is presented, featur-

* Corresponding author: Guoxiang Song (2023200720@aust.edu.cn).

ing a fractal circular configuration and exhibits an impedance bandwidth extending to 9.33 GHz. In [21], a four-port MIMO antenna design is introduced, incorporating two vertical metal barriers and inverted L-shaped stubs, aimed at enhancing the isolation among the antenna's ports. The method of opening slots or adding branches is generally used to solve the problems of narrow antenna bandwidth and poor decoupling effect [23–33]. Ref. [28] presents a four-port flexible MIMO antenna that consists of a circular ring and a T-shaped truncated line. The decoupling structure of this antenna consists of a rectangular truncated line, four open horizontal straplines, and two vertical straplines connecting to the grounding layer to achieve 22.5 dB isolation. Ref. [30] proposes a four-cell MIMO antenna using a half-cut miniaturization method to conceptualize an elliptical four-quadrant radiator with a C-shaped protruding ground plane as a quasi-monopole UWB antenna with a very compact size of only 18×11 mm^2. Ref. [33] presents two configurations of four-port MIMO antennas, where the antenna consists of an F-shaped patch and a mushroom-shaped defective floor, with U-shaped slots in the patch to obtain 25 dB of isolation. Ref. [34] presents a UWB-MIMO antenna with WLAN suppression characteristics, where the antenna trapping characteristics are realized by a helical electromagnetic bandgap. Ref. [35] proposes a two-port UWB-MIMO antenna with a mushroom-shaped Electromagnetic Band Gap (EBG) structure in the floor, where the trapping characteristics are achieved by opening U-shaped and L-shaped slots. Nonetheless, the aforementioned antenna designs presented in the literature suffer from certain limitations, notably including large physical dimensions, suboptimal decoupling performance, and limited bandwidth characteristics.

This paper presents the design of a compact UWB MIMO antenna aimed at enhancing port isolation. This is achieved through the incorporation of a T-shaped ground structure featuring cross slots, thereby augmenting the isolation between antenna ports. The designed antenna operates in the frequency range of $2.75 \sim 14.8$ GHz. The subsequent sections of this paper are organized as follows. Section 2 elaborates on the design methodology employed for the UWB antenna. Section 3 delineates various performance metrics derived from antenna simulations and measurements. Section 4 juxtaposes the findings with relevant references, and finally, Section 5 encapsulates the paper with a summary.

2. PROPOSED ANTENNA DESIGN

2.1. Structure of MIMO Antenna

Figure 1 depicts the configuration of the designed dual-port racket-shaped UWB antenna. This paper introduces a highly compact UWB MIMO antenna measuring 25 mm × 36 mm in size. The antenna is fabricated on a substrate with a thickness of 1.6 mm composed of standard FR4 material featuring a dielectric constant (ε_r) of 4.4 and a loss tangent (tanδ) of 0.02. The substrate of this material is lossy which is related to the thickness of the substrate. The thickness of the proposed antenna in this paper is 1.6 mm, which has the property of low profile which reduces the loss to some extent. The antenna

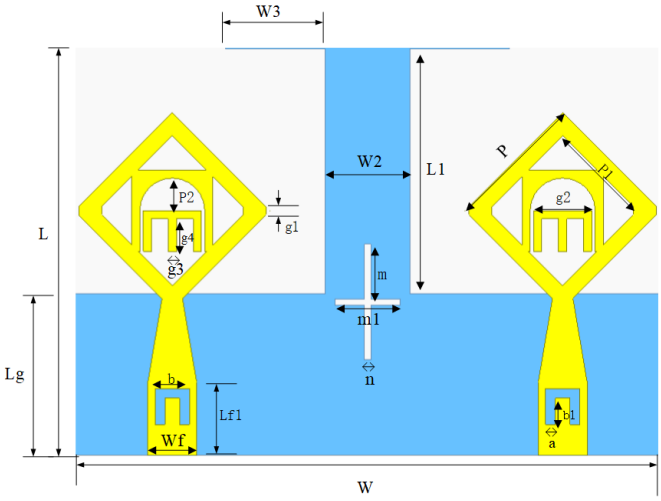

FIGURE 1. UWB MIMO antenna structure.

comprises two symmetrically positioned radiating patches atop a substrate, with the feed mechanism implemented via a microstrip line configuration. Loading the E-shaped patch at the center of the antenna changes the direction of current flow and improves isolation between ports. A U-shaped slot in the microstrip line of the antenna causes the S_{11} curve of the antenna to drop, which improves the bandwidth of the antenna. The introduction of the U-shaped slot also excites the antenna to resonate at 5.28 GHz. The dimensions of the U-shaped slot can be calculated with more Equations (1) and (2), where C is the electromagnetic wave propagation velocity, f_c the resonant frequency of 5.28 GHz, ε_{eff} the effective dielectric constant, ε_r the relative dielectric constant, h the thickness of the substrate, and W the width of the substrate. The separation distance between the two ports measures 24 mm. The T-shaped floor principle, aimed at enhancing antenna isolation, mirrors the resonator concept posited in [22]. The proposed antenna has cross slots based on the existing T-shaped decoupling structure [9, 21, 25], which improves the decoupling effect of the antenna. The antenna current flow can be blocked, which in turn reduces the mutual influence between the two ports.

$$b + 2 \times b_1 = \frac{C}{4 f_c \sqrt{\varepsilon_{eff}}} \tag{1}$$

$$\varepsilon_{eff} = \frac{\varepsilon_r + 1}{2} + \frac{\varepsilon_r - 1}{2} \left(1 + 12 \frac{h}{w}\right)^{-\frac{1}{2}} \tag{2}$$

Comprising two symmetrically positioned radiating patches and a substrate, the antenna employs a microstrip line for feed implementation. On the reverse side of the substrate, a T-shaped flawed floor is integrated, accompanied by a cross slot, further enhancing the antenna's decoupling capability. The structural dimensions of the designed UWB antenna are shown in Table 1.

2.2. Design Evolution Stages of the MIMO Antenna

The shape of the floor is continuously improved to enable the design of UWB MIMO antennas with good bandwidth and de-

TABLE 1. Dimensions of the proposed MIMO antenna structure.

parameters	W	L	L_g	L_1	L_{f1}	W_f	g_1	g_2	g_3	g_4	W_2
Value (mm)	36	25	9.9	15	4.5	3	0.5	3.6	0.5	2	5.2
parameters	W_3	P	P_1	P_2	a	b	b_1	m	m_1	n	
Value (mm)	6.1	8.5	6.5	5	0.6	2.1	1.6	7.1	4	0.4	

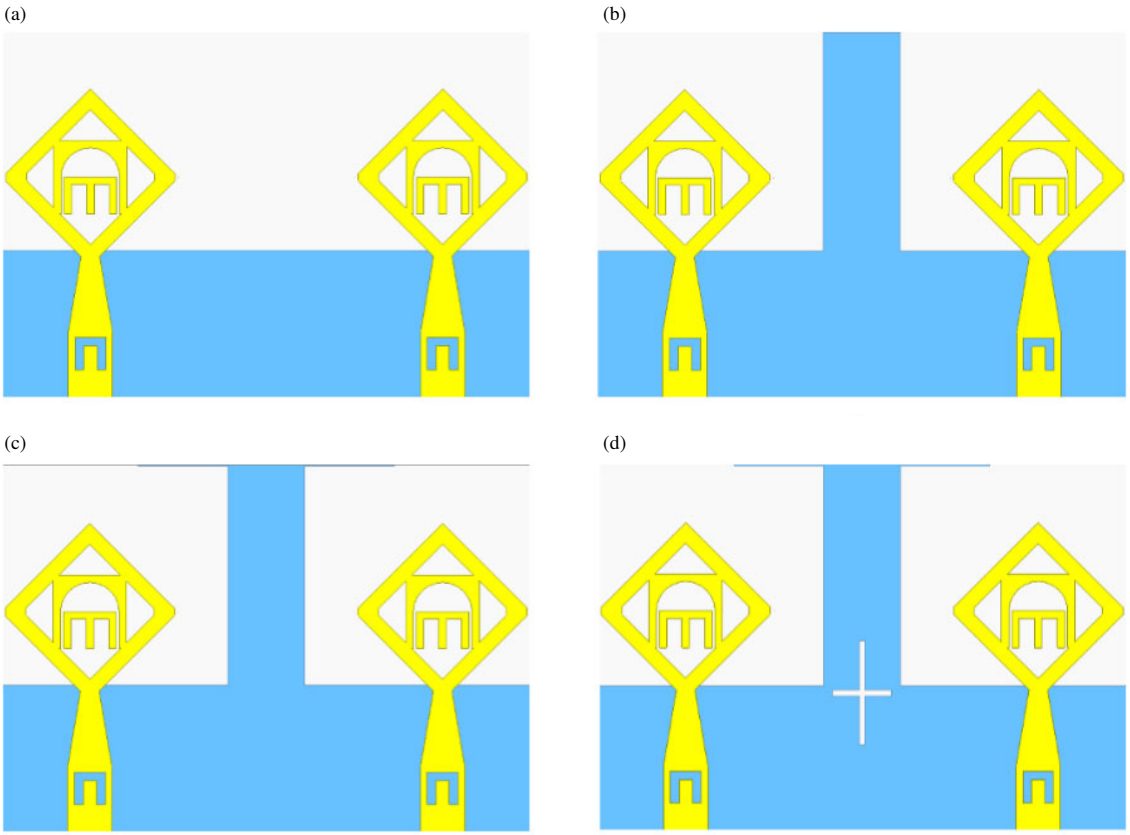

FIGURE 2. Design process of UWB MIMO antenna: (a) Ant1, (b) Ant2, (c) Ant3, (d) Ant4.

coupling. The design process of the antenna is shown in Figure 2.

As shown in Figure 2(a), the first antenna employs a conventional rectangular flawed ground structure. Since no decoupling structure is used, the isolation of the two ports of the antenna is poor, with S_{12} above -10 dB at the low-frequency position, and the antenna has a narrow bandwidth and can only operate in the $4.8 \sim 14.5$ GHz frequency range. As shown in Figure 2(b), the second antenna introduces rectangular extensions on the ground plane based on the design of the first antenna. The added rectangular branches impede the flow of current between the two ports, realizing a better decoupling effect. Moreover, the bandwidth of the antenna is greatly widened so that the antenna can work in the frequency range of $3.02 \sim 14.8$ GHz. The third antenna employs a T-shaped ground plane, facilitating improved decoupling between adjacent antennas. Furthermore, the bandwidth is expanded. Illustrated in Figure 2(d), depicting the proposed antenna configuration, a cross-shaped slot is incised into the base plate of antenna 3, thereby enhancing the antenna's decoupling effect, with S_{12} dropping below -20 dB across nearly the entire frequency spectrum ($2.74 \sim 14.8$ GHz). As demonstrated in Figure 3(a), the ultimate antenna configuration is distinguished by UWB, featuring an impedance bandwidth spanning $2.74 \sim 14.8$ GHz. As depicted in Figure 3(b), the optimization of isolation between the antenna's dual ports accompanies ongoing structural enhancements. Ultimately, the antenna attains over 20 dB of isolation across most of the frequency bands.

2.3. Antenna Parameter Analysis

The dimensions of the T-shaped floor can have a great impact on the performance of the antenna, and parameters L_1 and W_3 are optimized using HFSS software to achieve the best performance of the antenna. As shown in Figure 4(a), the impedance bandwidth of the antenna will change with the change of L_1, and as L_1 increases, the S_{11} curve will move downward in

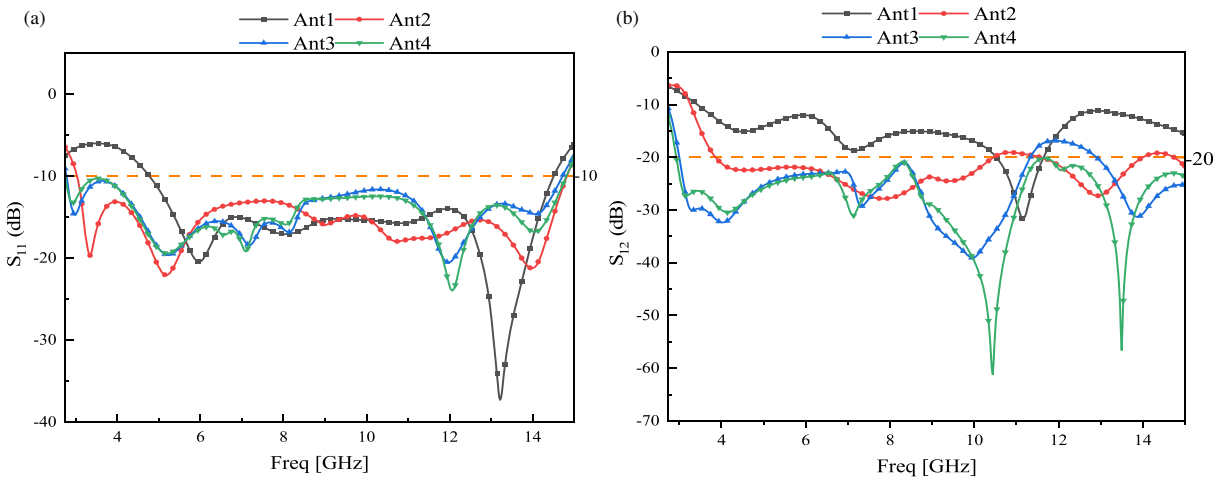

FIGURE 3. Simulation results for four antennas: (a) S_{11}, (b) S_{12}.

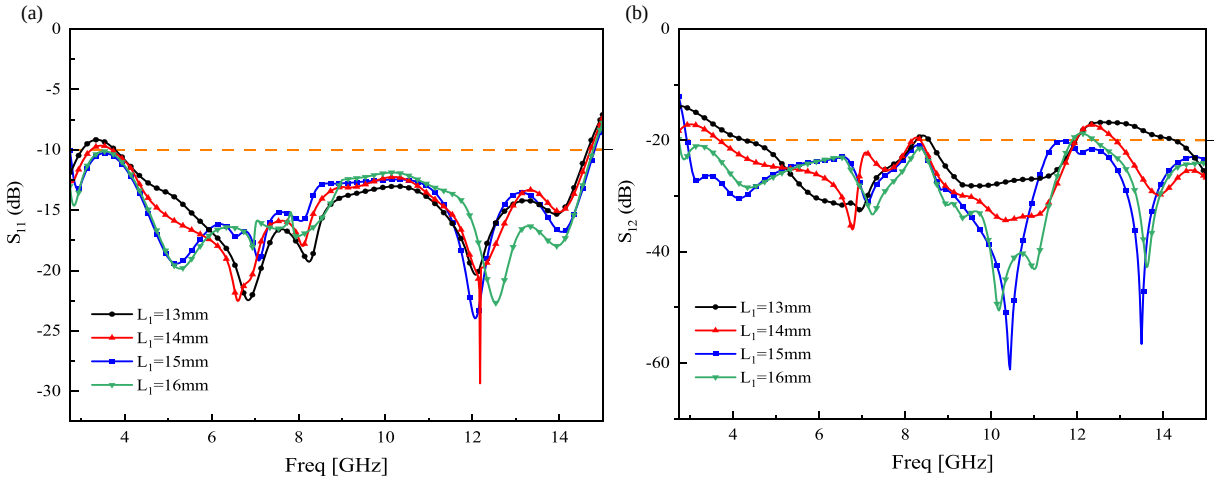

FIGURE 4. Effect of L_1 parameters on antennas: (a) S_{11}, (b) S_{12}.

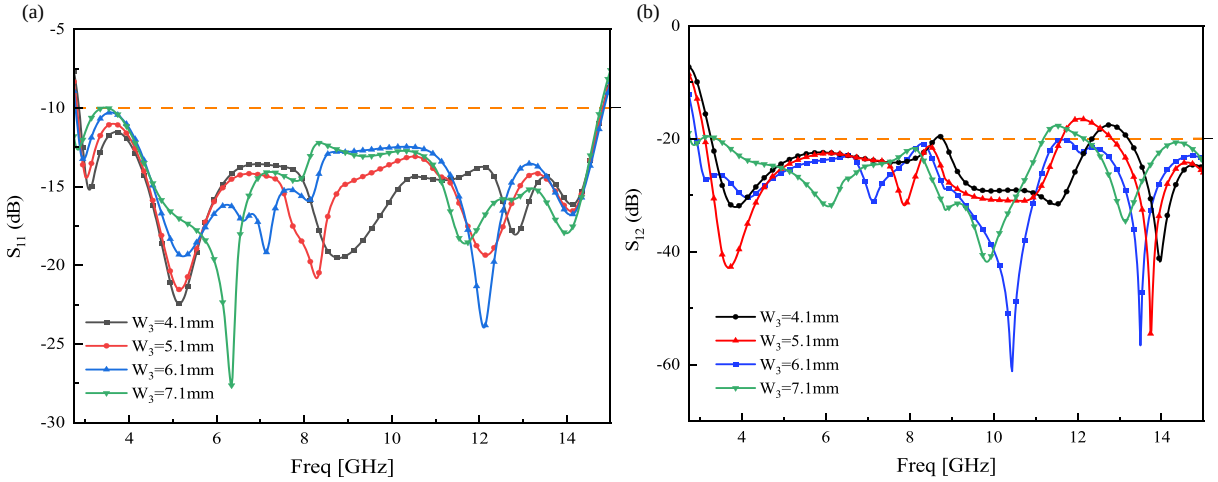

FIGURE 5. Effect of W_3 parameters on antennas: (a) S_{11}, (b) S_{12}.

the low-frequency position, and the bandwidth of the antenna increases with it. As shown in Figure 4(b), the value of L_1 also affects the isolation between the antenna ports, and the antenna has a good decoupling effect and a wide bandwidth when the value of L_1 is 15 mm. As shown in Figure 5(a), W_3 does not affect the antenna bandwidth significantly, whereas in Figure 5(b), W_3 has a significant effect on the isolation between

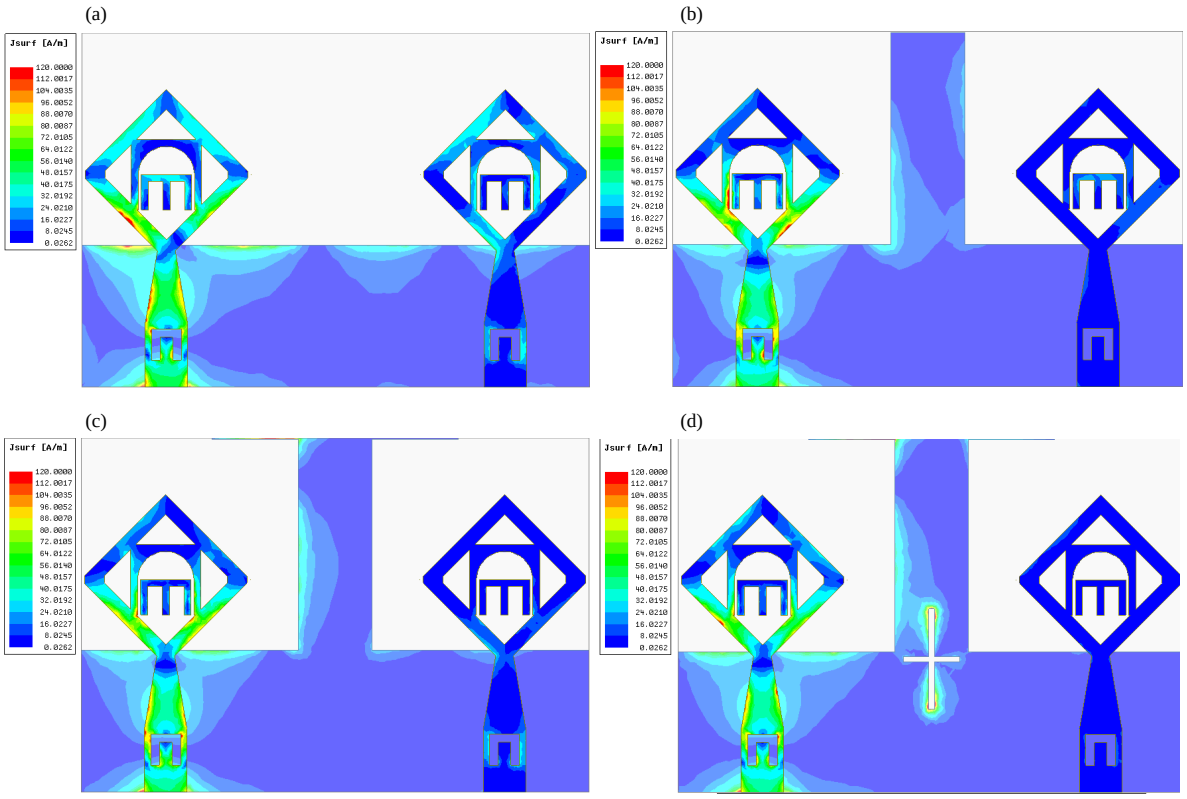

FIGURE 6. Surface currents for four floor-structured antennas: (a) Ant1, (b) Ant2, (c) Ant3, (d) Ant4.

the ports, and at a value of 6.1 mm for W_3 the antenna has good bandwidth and isolation.

2.4. Antenna Current Analysis

Figure 6 illustrates the surface current profiles of the four antennas, aimed at enhancing the decoupling effect of the MIMO antenna through an analysis of their surface currents. As depicted in Figure 6(a), the antenna employs a rectangular flawed ground plane and is excited at port 1. Simulation utilizing HFSS software reveals a substantial amount of current coupled into port 2. In Figure 6(b), a rectangular isolation strip is added in the middle part, and there is only a small amount of current in port 2. In Figure 6(c), a T-shaped floor is used, and only a small amount of current is coupled into port 2. Ultimately, the structure of the floor in Figure 6(d) is further improved by using a T-shaped floor structure as a whole with cross slots in the floor. The current in port 2 reaches a minimum, and the decoupling effect reaches an optimum. Therefore, the antenna finally adopts the floor structure in Figure 6(d), in which the T-shaped floor blocks the current flow between the ports, thus realizing a high isolation effect.

3. RESULTS AND DISCUSSION

3.1. S-Parameters

MIMO antennas are simulated utilizing HFSS software. To validate the practical performance of the antenna, the antenna model undergoes machining, and the resulting prototype is depicted in Figure 7. Antenna testing was conducted employing an Agilent N52235A vector network analyzer, with the test setup illustrated in Figure 8. The frequency range covered by the antenna, as depicted in Figure 9, spans from 2.74 to 14.8 GHz, covering the UWB of 3.1 $\sim$ 10.6 GHz. Furthermore, the S_{12} parameter of the antenna remains below -20 dB within the UWB, indicating a favorable isolation effect. Although some errors exist between the S_{11} and S_{12} measurements and simulations depicted in Figure 9, they exhibit overall similarity, and the antenna's overall performance remains consistent. In addition, the simulated and measured errors may be caused by the processing and testing environments.

3.2. Radiation Properties

The radiation direction maps of the UWB-MIMO antenna in the YOZ and XOZ directions were measured in a microwave darkroom. Five resonance points of the antenna were selected for the measurements. The results are shown in Figure 10. From Figure 10(a), it can be seen that the antenna achieves almost omnidirectional radiation in the YOZ and XOZ directions at 2.9 GHz frequency. From Figure 10(b), it can be found that the antenna achieves omnidirectional radiation in the YOZ plane at 5.28 GHz frequency, while for the XOZ plane, the antenna has the strongest radiation gain at 0° and 175°, and the antenna has good radiation characteristics. As shown in Figure 10(c), the antenna is almost omnidirectional in the YOZ direction at 7.2 GHz, and the radiation gain is maximum at 205° and 330°, while in the XOZ direction, the antenna orienta-

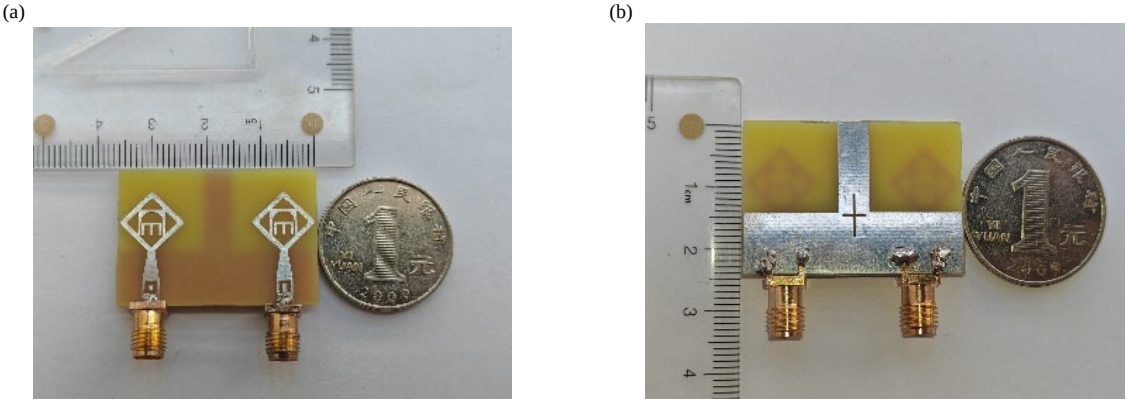

FIGURE 7. Fabrication prototype of MIMO antenna: (a) Front of the antenna, (b) back side of the antenna.

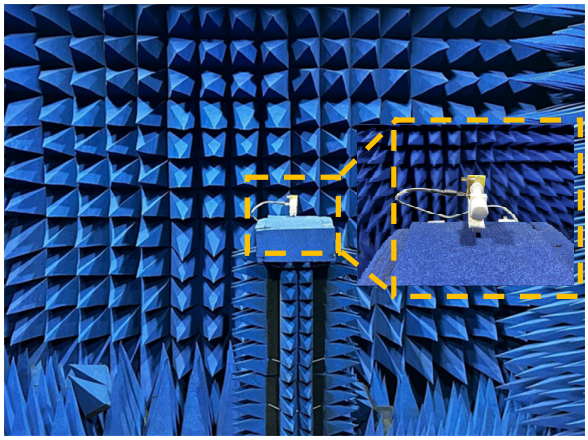

FIGURE 8. Antenna test environment.

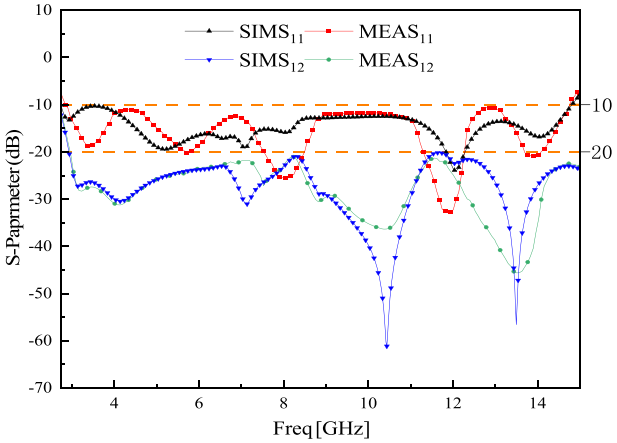

FIGURE 9. Simulated and measured S-parameters.

tion map shows an elliptical shape, and the radiation gain is maximum at 35° and 205° directions. At 12.1 GHz, the maximum radiation direction of YOZ is mainly distributed between 30° $\sim$ 310° and 180° $\sim$ 240°. The maximum radiation direction of XOZ is mainly distributed between 30° to 330° and 150° to 270°. At 14 GHz, the maximum radiation directions on the YOZ surface are located at 15°, 90°, 180°, and 270°. For the XOZ surface, the direction map shows almost omnidirectionality.

Figure 11 displays the maximum gain and radiation efficiency of the MIMO antenna. The maximum value of the peak gain of the antenna reaches 5.4 dBi, and the radiation efficiency of the antenna ranges from 73% to 96%. In the frequency range of 2.74 $\sim$ 11 GHz, the antenna's radiation efficiency exceeds 90%, which indicates that most of the energy of the antenna is radiated out, and the antenna has a very good radiation performance.

3.3. MIMO Antennas Performance

3.3.1. ECC and DG

The correlation envelope coefficient (ECC) is the correlation of the received signal amplitude between different antenna units and is used as a parameter index to assess the diversity performance and coupling performance of MIMO multi-antenna systems. A smaller value of ECC indicates a lesser inter-antenna cell influence and a better performance of the MIMO antenna. In general, for the antenna to function normally, the ECC value must be smaller than 0.5. The antenna's S-parameters can be used to compute the ECC. The formula for ECC is shown below:

$$\mathrm{ECC} = \frac{\left|S_{11}^{*}S_{12} + S_{21}^{*}S_{22}\right|^{2}}{\left(1 - \left|S_{11}\right|^{2} - \left|S_{21}\right|^{2}\right)\left(1 - \left|S_{22}\right|^{2} - \left|S_{12}\right|^{2}\right)} \tag{3}$$

DG is another performance metric for MIMO antennas, which can be calculated by ECC, and the closer its value is to 10 dB, the better the antenna works. The calculation formula is shown below:

$$\mathrm{DG} = 10 \times \sqrt{1 - |\mathrm{ECC}|} \tag{4}$$

As shown in Figure 12, the maximum value of antenna ECC is about 0.03, which is less than 0.005 at most of the frequencies. The minimum value of antenna DG reaches 9.84 dB, and the antenna has good diversity performance.

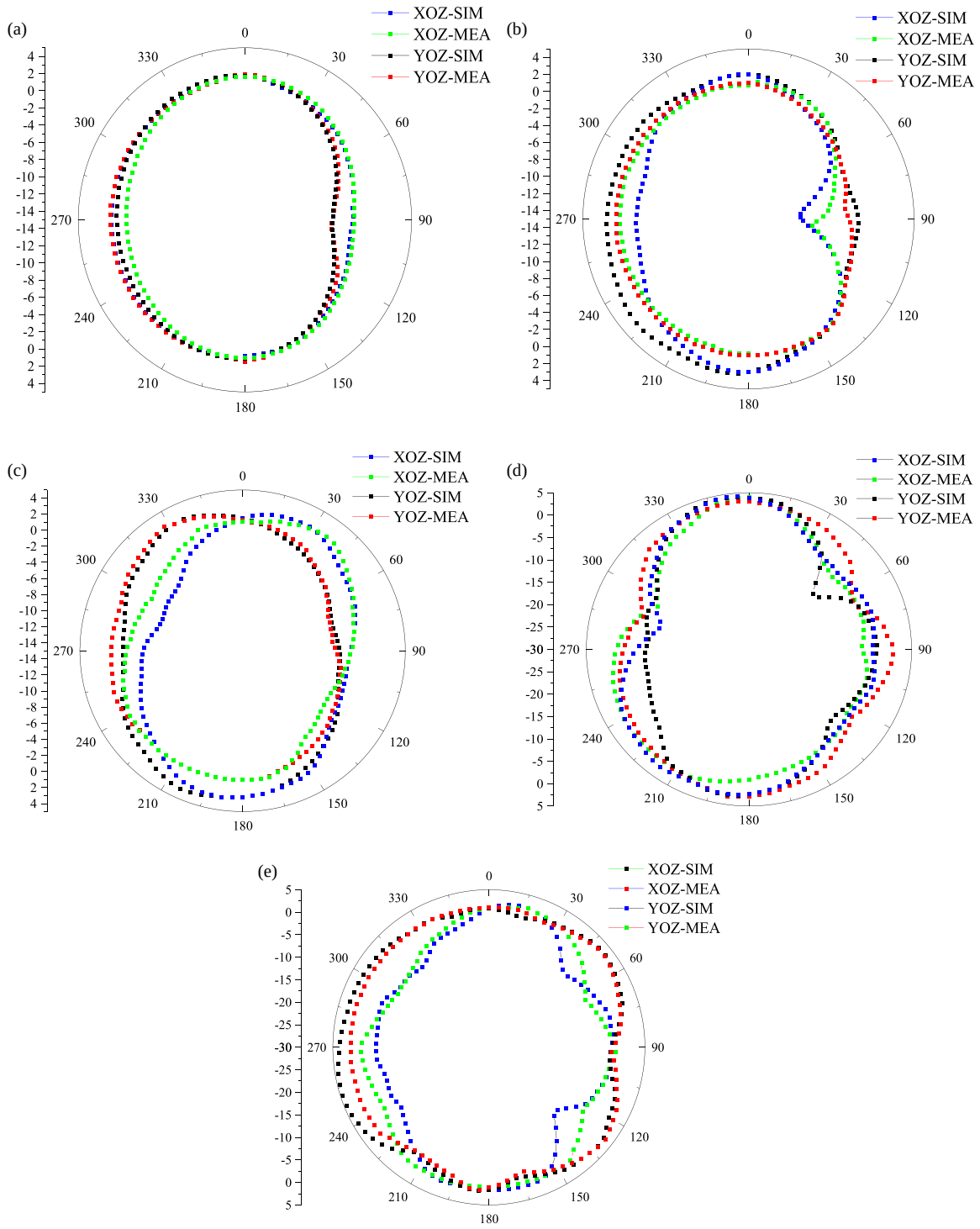

FIGURE 10. Simulated and measured orientation diagrams: (a) 2.9 GHz, (b) 5.28 GHz, (c) 7.2 GHz, (d) 12.1 GHz, (e) 14 GHz.

3.3.2. TARC and CCL

TARC is an important performance metric for MIMO antennas. It indicates the effective bandwidth of the MIMO antenna for simultaneous excitation of multiple ports, which can be calculated using S-parameters. Generally speaking, an antenna is considered to be performing well if its TARC value in the working band is less than -10 dB. The TARC for a dual-port MIMO antenna can be computed with the following formula:

$$\mathrm{TARC} = \sqrt{\frac{(S_{11}+S_{12})^2 + (S_{21}+S_{22})^2}{2}} \tag{5}$$

Figure 13 shows the TARC of the antenna, which is below -20 dB over the operating band, indicating that the antenna decouples well.

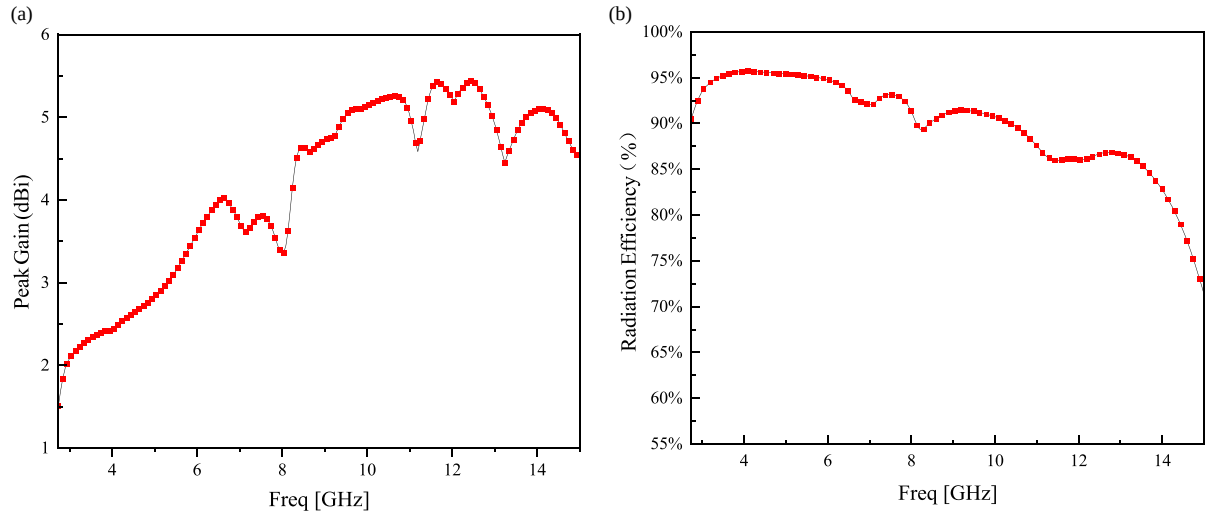

FIGURE 11. Peak gain and radiation efficiency of the antenna: (a) Peak gain, (b) radiation efficiency.

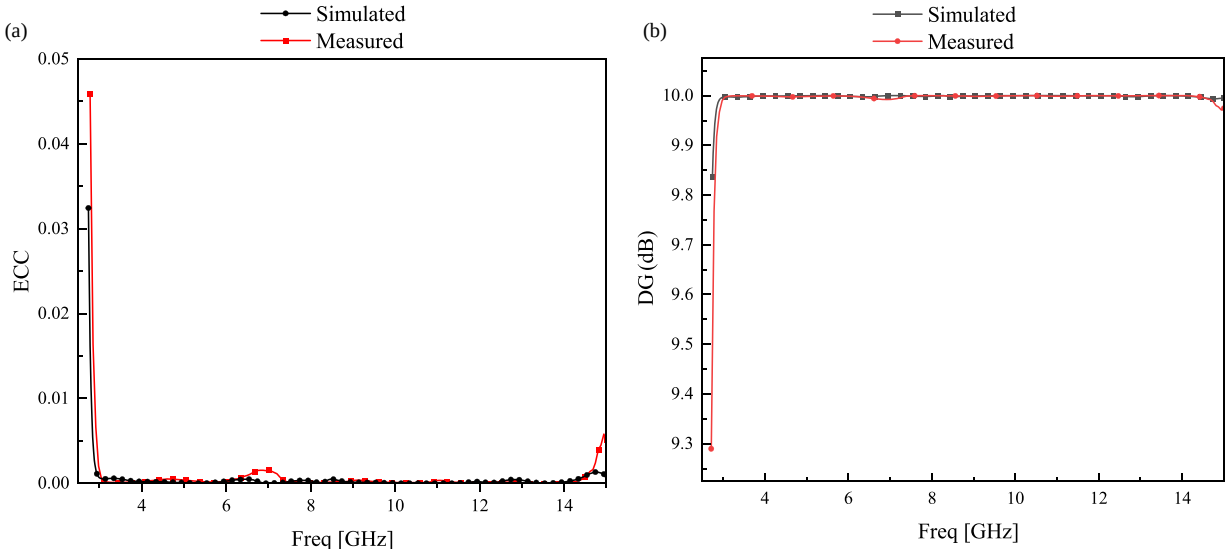

FIGURE 12. ECC and DG of the antenna: (a) ECC, (b) DG.

TABLE 2. Comparison of the proposed antenna with several existing antennas.

Ref.	Size (mm^2)	Bandwidth (GHz)	Isolation (dB)	ECC	Radiation efficiency (%)
[1]	62.5×60.5	3.5–11	> 20	< 0.01	70–90
[9]	30×18	4.3–15.63	> 20	< 0.0075	85–93
[10]	24×24	2.9–10.6	> 15	< 0.01	-
[11]	52×26	2.3–11.5	> 16	< 0.012	-
[12]	90×90	2.77–12	> 15	< 0.1	75–85
[15]	40×40	3–13.5	> 15	< 0.4	89–95
[18]	48×35	2–12.1	> 20	< 0.07	80–90
[19]	90×90	2.77–12	> 15	< 0.1	75–82
[20]	40×40	3–13.5	> 15	< 0.4	89–95
This work	25×36	2.74–14.8	> 20	< 0.0325	74–95.7

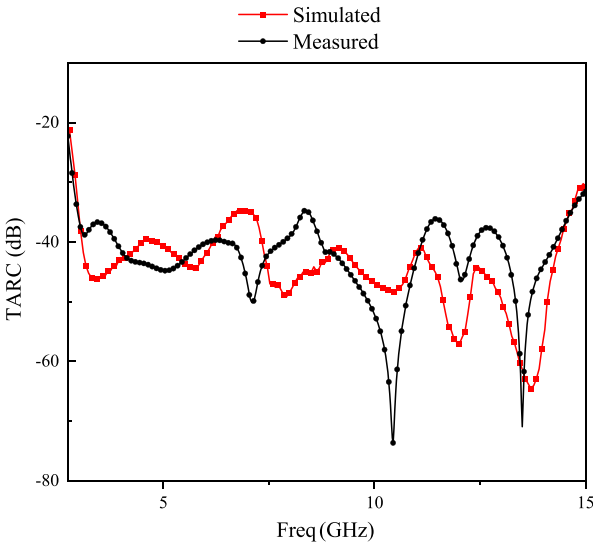

FIGURE 13. Simulated and measured TARCs.

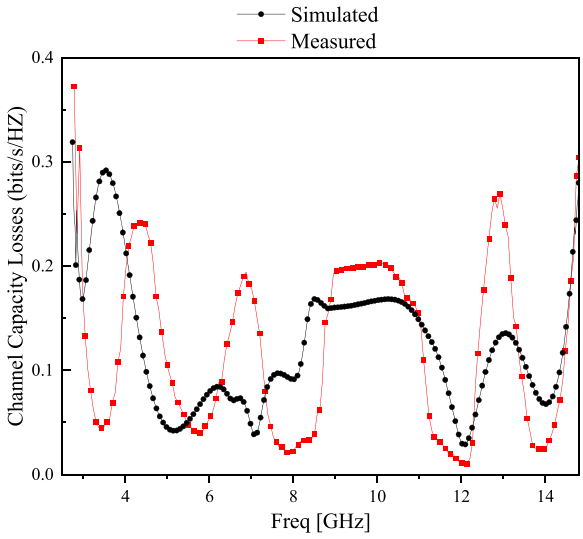

FIGURE 14. Simulated and measured CCLs.

CCL is also an important parameter in the MIMO antenna, generally speaking, CCL less than 0.4 bit/s/Hz meets the design requirements of a MIMO antenna. It is calculated from the S-parameters according to Equations (6), (7), (8), (9). The simulated and measured CCLs are shown in Figure 14.

$$\mathrm{CCL} = -\log_2 \det\left(\alpha^R\right) \tag{6}$$

$$\alpha^R = \begin{bmatrix} \alpha_{11} & \alpha_{12} \\ \alpha_{21} & \alpha_{22} \end{bmatrix} \tag{7}$$

$$\begin{aligned} \alpha_{11} &= 1 - \left(|S_{11}|^2 + |S_{12}|^2\right); \\ \alpha_{12} &= -S_{11} * S_{12} - S_{21} * S_{22} \\ \alpha_{22} &= 1 - \left(|S_{22}|^2 + |S_{21}|^2\right); \\ \alpha_{21} &= -S_{22} * S_{21} - S_{12} * S_{11} \end{aligned} \tag{8, 9}$$

4. COMPARISON WITH EXISTING ANTENNAS

Table 2 shows a comparison between the antenna proposed in this paper and several existing antennas concerning size, bandwidth, isolation, ECC, and radiation efficiency. The suggested antenna has a smaller size than [1, 11, 12, 15, 18–20]. The bandwidth of the antenna is wider than [1, 10–12, 15, 18–20], and the isolation of the antenna is higher than [10–12, 15, 19, 20]. In addition, the antenna has a lower ECC than [12, 15, 18–20]. Moreover, the antenna has good radiation efficiency up to more than 95%. Therefore, the proposed antenna has better performance and meets the design requirements of the UWB MIMO antenna.

5. CONCLUSION

In this paper, a high-isolation UWB MIMO antenna is designed. The antenna consists of two racket-shaped metal patches and adopts an improved T-shaped defective floor structure with cross slots on the T-shaped floor to realize the decoupling between the antenna ports, and the isolation effect is almost always above 20 dB, covering the UWB (3.1 $\sim$ 10.6 GHz). The antenna has multiple resonance points to expand the impedance bandwidth of the antenna, and the antenna operates in the range of 2.74 $\sim$ 14.8 GHz. This range includes commonly used frequency bands, such as 5G (3.3 $\sim$ 3.6 GHz/4.8 $\sim$ 5.0 GHz), WiMAX (3.4 $\sim$ 3.69 GHz), WLAN (5.15 $\sim$ 5.35 GHz), and satellite communications in the C-band (4 $\sim$ 8 GHz), X-band (8 $\sim$ 12 GHz).

ACKNOWLEDGEMENT

This work was supported in part the Natural Science Research Project of Anhui Educational Committee under No. 2022AH051583 and No. 2022AH052138, in part by the Anhui Province Graduate Academic Innovation Project under grant No. 2023xscx074.

REFERENCES

[1] Abdelghany, M. A., M. F. A. Sree, A. Desai, and A. A. Ibrahim, "4-port octagonal shaped MIMO antenna with low mutual coupling for UWB applications," *Computer Modeling in Engineering & Sciences*, Vol. 136, No. 2, 1999–2015, 2023.

[2] Jayant, S., G. Srivastava, and S. Kumar, "Quad-port UWB MIMO footwear antenna for wearable applications," *IEEE Transactions on Antennas and Propagation*, Vol. 70, No. 9, 7905–7913, 2022.

[3] Addepalli, T., J. B. Kamili, S. Boddu, R. Manda, A. Nella, and B. K. Kumar, "A 4-element crescent shaped two-sided MIMO antenna for UWB, X and Ku band wireless applications," *Wireless Networks*, Vol. 29, No. 8, 3333–3348, 2023.

[4] Ren, W., Z. Wang, M. Yang, J. Zhou, and W. Nie, "Design of a simple four-port UWB-MIMO antenna based on a fan-shaped isolator," *Progress In Electromagnetics Research M*, Vol. 126, 117–126, 2024.

[5] Pakala, R. and D. Ramakrishna, "Mutual coupling reduction in UWB-MIMO antenna using circular slot EBG structure,"

Progress In Electromagnetics Research M, Vol. 119, 177–188, 2023.

[6] Naktong, W. and A. Ruengwaree, "Four-port rectangular monopole antenna for UWB-MIMO applications," *Progress In Electromagnetics Research B*, Vol. 87, 19–38, 2020.

[7] Kolangiammal, S., L. Balaji, and M. Mahdal, "A compact planar monopole UWB MIMO antenna for short-range indoor applications," *Sensors*, Vol. 23, No. 9, 4225, 2023.

[8] Kumar, P., S. Pathan, S. Vincent, O. P. Kumar, N. Yashwanth, P. Kumar, P. R. Shetty, and T. Ali, "A compact quad-port UWB MIMO antenna with improved isolation using a novel mesh-like decoupling structure and unique DGS," *IEEE Transactions on Circuits and Systems II: Express Briefs*, Vol. 70, No. 3, 949–953, 2023.

[9] Mu, W., H. Lin, Z. Wang, C. Li, M. Yang, W. Nie, and J. Wu, "A flower-shaped miniaturized UWB-MIMO antenna with high isolation," *Electronics*, Vol. 11, No. 14, 2190, 2022.

[10] Dhanalakshmi, K. M., G. Kavya, and S. Rajkumar, "A monopole polarisation diversity antenna for high density packaging MIMO applications," *Microelectronics International*, Vol. 41, No. 2, 75–81, 2023.

[11] Kiani, S. H., H. S. Savci, M. E. Munir, A. Sedik, and H. Mostafa, "An ultra-wide band MIMO antenna system with enhanced isolation for microwave imaging applications," *Micromachines*, Vol. 14, No. 9, 1732, 2023.

[12] Ahmed, B. T., "High isolation compact UWB MIMO antennas," *Wireless Personal Communications*, Vol. 128, No. 4, 3003–3029, 2023.

[13] Addepalli, T., K. V. Babu, T. Vidyavathi, R. Manda, and B. K. Kumar, "Design and analysis of nonagonal patch unite with rectangular shaped 4-element UWB-MIMO antenna for portable wireless device applications," *Analog Integrated Circuits and Signal Processing*, Vol. 114, No. 3, 459–473, 2023.

[14] Suresh, A. C., T. S. Reddy, B. T. P. Madhav, S. Das, S. Lavadiya, A. D. Algarni, and W. El-Shafai, "Investigations on stub-based UWB-MIMO antennas to enhance isolation using characteristic mode analysis," *Micromachines*, Vol. 13, No. 12, 2088, 2022.

[15] Khan, A., S. Bashir, S. Ghafoor, H. Rmili, J. Mirza, and A. Ahmad, "Isolation enhancement in a compact four-element MIMO antenna for ultra-wideband applications," *Computers, Materials & Continua*, Vol. 75, No. 1, 911–925, 2023.

[16] Nan, J.-C., M.-H. Wang, M.-M. Gao, and J. Liu, "Miniaturized inverted ultra-wideband multiple-input multiple-output antenna with high isolation," *Electronics Letters*, Vol. 57, No. 3, 100–102, 2021.

[17] Fadehan, G. A., Y. O. Olasoji, and K. B. Adedeji, "Mutual coupling effect and reduction method with modified electromagnetic band gap in UWB MIMO antenna," *Applied Sciences*, Vol. 12, No. 23, 12358, 2022.

[18] Essid, C., C. Abdelhamid, F. A. Almalki, O. Ali, and H. Sakli, "New MIMO antenna with filtration for the future multiuser systems in satellite communications," *Wireless Communications and Mobile Computing*, Vol. 2022, No. 1, 1040333, 2022.

[19] Alharbi, A. G., U. Rafique, S. Ullah, S. Khan, S. M. Abbas, E. M. Ali, M. Alibakhshikenari, and M. Dalarsson, "Novel MIMO antenna system for ultra wideband applications," *Applied Sciences*, Vol. 12, No. 7, 3684, 2022.

[20] Khan, A. A., S. A. Naqvi, M. S. Khan, and B. Ijaz, "Quad port miniaturized MIMO antenna for UWB 11 GHz and 13 GHz frequency bands," *AEU — International Journal of Electronics and Communications*, Vol. 131, 153618, 2021.

[21] Ahmed, B. T., "High isolation compact UWB MIMO antennas," *Wireless Personal Communications*, Vol. 128, No. 4, 3003–3029, 2023.

[22] Roshani, S. and H. Shahveisi, "Mutual coupling reduction in microstrip patch antenna arrays using simple microstrip resonator," *Wireless Personal Communications*, Vol. 126, No. 2, 1665–1677, 2022.

[23] Fiser, O., V. Hruby, J. Vrba, T. Drizdal, J. Tesarik, J. V. Jr, and D. Vrba, "UWB bowtie antenna for medical microwave imaging applications," *IEEE Transactions on Antennas and Propagation*, Vol. 70, No. 7, 5357–5372, 2022.

[24] Saleh, S., W. Ismail, I. S. Z. Abidin, M. H. Jamaluddin, M. H. Bataineh, and A. S. Al-Zoubi, "Novel compact UWB Vivaldi nonuniform slot antenna with enhanced bandwidth," *IEEE Transactions on Antennas and Propagation*, Vol. 70, No. 8, 6592–6603, 2022.

[25] Li, W., L. Wu, S. Li, X. Cao, and B. Yang, "Bandwidth enhancement and isolation improvement in compact UWB-MIMO antenna assisted by characteristic mode analysis," *IEEE Access*, Vol. 12, 17 152–17 163, 2024.

[26] Sharma, M., T. Addepalli, R. Manda, T. Vidyavathi, and P. R. Kapula, "A detailed insight of 2×2 high isolation wideband dual notched band MIMO antenna with evolution initiated by theory of characteristics mode," *International Journal of Microwave and Wireless Technologies*, Vol. 15, No. 8, 1392–1411, 2023.

[27] Jetti, C. R., T. Addepalli, S. R. Devireddy, G. K. Tanimki, A. J. A. Al-Gburi, Z. Zakaria, and P. Sunitha, "Design and analysis of modified U-shaped four element MIMO antenna for dual-band 5G millimeter wave applications," *Micromachines*, Vol. 14, No. 8, 1545, 2023.

[28] Shariff, B. G. P., T. Ali, P. R. Mane, M. G. N. Alsath, P. Kumar, S. Pathan, A. A. Kishk, and T. Khan, "Design and measurement of a compact millimeter wave highly flexible MIMO antenna loaded with metamaterial reflective surface for wearable applications," *IEEE Access*, Vol. 12, 30 066–30 084, 2024.

[29] Dash, S. K. K., Q. S. Cheng, T. Khan, M. V. Yadav, and L. Wang, "5G millimeter-wave MIMO DRAs with reduced mutual coupling," *Microwave and Optical Technology Letters*, Vol. 66, No. 1, e33982, 2024.

[30] Shome, P. P., T. Khan, A. A. Kishk, and Y. M. M. Antar, "Quad-element MIMO antenna system using half-cut miniaturized UWB antenna for IoT-based smart home digital entertainment network," *IEEE Internet of Things Journal*, Vol. 10, No. 20, 17 964–17 976, 2023.

[31] Tiwari, R. N., V. Kaim, P. Singh, T. Khan, and B. K. Kanaujia, "Semi-flexible diversified circularly polarized millimeter-wave MIMO antenna for wearable biotechnologies," *IEEE Transactions on Antennas and Propagation*, Vol. 71, No. 5, 3968–3982, 2023.

[32] Modak, S., S. Daasari, P. P. Shome, and T. Khan, "Switchable/tunable band-notched characteristics in UWB and UWB-MIMO antennas: A comprehensive review," *Wireless Personal Communications*, Vol. 128, No. 3, 2131–2154, 2023.

[33] Modak, S., T. Khan, T. A. Denidni, and Y. M. M. Antar, "Miniaturized self-isolated UWB MIMO planar/cuboidal antenna with dual X-band interference rejection," *AEU — International Journal of Electronics and Communications*, Vol. 143, 154020, 2022.

[34] Modak, S. and T. Khan, "Cuboidal quad-port UWB-MIMO antenna with WLAN rejection using spiral EBG structures," *International Journal of Microwave and Wireless Technologies*, Vol. 14, No. 5, 626–633, 2022.

[35] Modak, S. and T. Khan, "A slotted UWB-MIMO antenna with quadruple band-notch characteristics using mushroom EBG structure," *AEU — International Journal of Electronics and Communications*, Vol. 134, 153673, 2021.